Dalton Transactions

ROYAL SOCIETY OF CHEMISTRY

PAPER

View Article Online
View Journal | View Issue

Cite this: *Dalton Trans.*, 2025, **54**, 649

Highly selective organo-gallium hydroxamate mediated inhibition of antibiotic resistant *Klebsiella pneumoniae*†

Rebekah N. Duffin, Jenisi T. A. Kelderman, Megan E. Herdman and Philip C. Andrews *

Five complexes of gallium derived from hydroxamic acids have been synthesised, characterised, and their anti-bacterial activity and mammalian cell toxicity established. These are three metal–organic complexes; $[Ga(BPHA)_3]$ **1**, $[Ga(BHA\text{-}H)_3]$ **2**, $[Ga(SHA\text{-}H_2)(SHA\text{-}H)_3]$ **3**, and two heteroleptic organometallic complexes $[GaMe_2(BPHA)]$ **4**, and $[GaMe(BHA\text{-}H)_2]$ **5**, along with the iron complex $[Fe(BPHA)_3]$ **6** (BPHA-H = *N*-benzoyl-*N*-phenylhydroxamic acid, BHA-H_2 = phenylhydroxamic acid, and SHA-H_3 = salicylhydroxamic acid). Solid-state structures of **1**, **4–6** were identified by single-crystal X-ray crystallography. Complexes **1** and **6** adopt an octahedral geometry at the metal centre, while the organometallic complexes **4** and **5** adopt, respectively, tetrahedral and trigonal bipyramidal geometry. The solution and solid-state chemistry of complex **3** was found to differ: the solution state is composed of an equilibrium mixture of the bis-complexed hydroximate–hydroxamate species and the homoleptic tris-hydroxamate species, with the solid state preferring the bis-complexed hydroximate–hydroxamate composition. The methyl gallium complexes **4** and **5** differed in their preferred composition with **4** forming the expected dimethyl hydroxamate complex while **5** stabilises as the methyl bis-hydroxamate complex. Complexes were tested for the anti-microbial activity against a series of Gram-positive and Gram-negative bacteria, with an emphasis on the Gram-negative *Klebsiella pneumoniae*. While the metal–organic complexes **1**, **2**, **3** and **6** showed little to no activity towards either the bacteria or mammalian cells, the alkyl gallium complexes **4** and **5** were found to have exceptional activity toward *K. pneumoniae* in RPMI-HS media with MIC values of 78 nM. Interestingly, $[GaMe_2(OH)]$ also showed significant activity with an MIC of 156 nM.

Received 28th August 2024,
Accepted 5th November 2024

DOI: 10.1039/d4dt02440k

rsc.li/dalton

Introduction

Klebsiella pneumoniae is a major opportunistic nosocomial pathogen of the *Enterobacteriaceae* family.[1] It is one of the ESKAPE bacteria, classified as nosocomial pathogens that exhibit multidrug resistance and virulence, with the remaining five encompassing *Enterococcus faecium*, *Staphylococcus aureus*, *Pseudomonas aeruginosa*, *Acinetobacter baumannii* and *Enterobacter* spp.[2] Typically *K. pneumoniae* is found in the flora of the mouth, skin and intestines. However, it often inhabits medical devices and high-touch surfaces, creating substantial infection risk for patients with compromised and weakened immune systems.[3] Biofilm formation on medical devices poses a major threat due to unintentional infection, especially in catheter patients.[4] For two main reasons *K. pneumoniae* infections tend to be chronic: biofilm formation provides a protective barrier *in vivo* toward host immune responses and antibiotics, and common nosocomial strains tend to display multidrug resistance due to the extended-spectrum β-lactamases (ESBL) or carbapenem exposure, causing difficulties in drug selection for treatment.[5–7]

K. pneumoniae, like many pathogens, have evolved sophisticated ways in which to either evade host immunity or inhibit it. For example: a thick capsule at the cell surface enables evasion of host phagocytosis by immune cells (*e.g.*, macrophages, neutrophils) in hypervirulent strains.[8,9] Furthermore, the evolution of bacterial efflux pumps to actively export antibiotics has led to the rapid development of antibiotic resistance. These efflux pumps are also able to remove host derived antimicrobial agents, such as antimicrobial peptides.[10]

Like most pathogens *K. pneumoniae* requires iron from exogenous sources. There are at least 12 distinctive transport

School of Chemistry, Monash University, Clayton, Melbourne, VIC 3800, Australia. E-mail: phil.andrews@monash.edu

† Electronic supplementary information (ESI) available. CCDC 2150403, 2150396, 2380238, 2380239, 2150393, 2330100, 2330099 and 2330101. For ESI and crystallographic data in CIF or other electronic format see DOI: https://doi.org/10.1039/d4dt02440k

systems for iron in *K. pneumoniae* found in four major categories: Ferrous transporters (FeO), ABC transporters, hemophore-based uptake, and siderophore uptake systems. Only the siderophore based systems and two of the ABC transporters are required for full virulency.[11] Siderophore mediated uptake is the major acquisition pathway for *K. pneumoniae*, utilising this high iron affinity transporter to obtain iron in the iron-poor environments of their mammalian hosts. Scarcity of iron tends to cause an increase in the production of these siderophores in an attempt to maintain a high degree of pathogenicity and homeostasis for further growth and infection. Hypervirulent strains also secrete a higher concentration of these siderophores in comparison to classical strains.[12–14] These siderophores generally contain carboxylate, catecholate, and hydroxamate functional groups as main metal chelation sites.

Gallium is known to mimic iron *in vivo.* Ga(III) binds to and is transported by similar proteins, including transferrin, lactoferrin and serum albumin. The main uptake pathway for Ga into cells has been shown to be mediated by transferrin receptors (TfR) but the very different redox chemistry, which requires reduction of Fe(III) to Fe(II) for TfR, indicates that the uptake processes are not exactly the same and that different non-TfR pathways are possible.[15]

As discussed, *K. pneumoniae* will up-regulate production of the siderophores aerobactin and enterobactin in iron-poor environments.[15,16] There is therefore the potential to exploit this nutritional requirement using gallium as an iron pathway inhibitor. The chemical similarities between Ga(III) and Fe(III) make it exceptionally difficult for bacteria to distinguish between the two, ultimately leading to uptake of gallium *via* siderophores and inhibition of redox-active pathways. This mechanistic pathway, the "Trojan Horse effect" is therefore the target of a variety of potential gallium-based therapeutics.[17,18] Deferoxamine is a polyfunctional siderophore mimic which is used therapeutically to treat iron overload in the body, primarily using hydroxamate chelation. Though there have been investigations into the antibacterial activity of Ga(III) deferoxamine complexes they were found to exhibit similar or higher toxicity than the parent Ga(III) salt, suggesting broad antimicrobial properties.[19] Beyond this there is only limited research into the structure and bio-activity of more simple gallium hydroxamate complexes.

Recently, we have shown that complexation with Ga(III) can reactivate previously inactive quinolone antibiotics in low iron environments. Importantly, the most active complexes had the organogallium [$GaMe_2$] moiety at their core. The complexes exhibited highly potent activity toward four antibiotic resistant strains of *K. pneumoniae* in RPMI media supplemented with 10% human AB serum,[20] much greater that their homoleptic [GaL_3] analogues. Similarly, a class of dimethyl gallium quinolinolates were also observed to be exceptional inhibitors of *K. pneumoniae* in reduced iron media,[21] and were again much superior to their tris-quinolinolate analogues. This hints at the uniqueness of the heteroleptic organogallium complexes compared with the traditional homoleptic salts and metal–organic complexes.

As such, our efforts have focussed in on the differences in the homoleptic and heteroleptic gallium complexes and the effect of lipophilicity, hydrolytic stability, protein exchange kinetics, and solubility in their biological activity.[20] This current study draws on this, and the role of hydroxamate chelation, in exploring the synthesis, characterisation and antibacterial activity of a range of gallium hydroxamate complexes.

Three structurally diverse hydroxamic acids; *N*-benzoyl-*N*-phenylhydroxamic acid (BPHA-*H*), phenylhydroxamic acid (BHA-H_2), and salicylhydroxamic acid (SHA-H_3), shown in Fig. 1, were used in the synthesis of three metal–organic gallium complexes and one iron complex [Ga(BPHA)$_3$] **1** [Ga(BHA-*H*)$_3$] **2**, and [Ga(SHA-H_2)(SHA-*H*)] **3**, [Fe(BPHA)$_3$] **6**, and two heteroleptic organometallic complexes, [$GaMe_2$(BPHA)] **4** and [GaMe(BHA-*H*)$_2$] **5**. These are shown in Fig. 2.

In addition to *K. pneumoniae*, the compounds were also analysed for their antibiotic activity against a range of Gram-positive and Gram-negative bacteria including methicillin resistant *S. aureus* (MRSA), vancomycin resistant *Enterococcus* (VRE), *E. coli*, *P. aeruginosa* and *A. baumannii.* Cytotoxicity toward mammalian control cells was also assessed and the selectivity index of the complexes calculated.

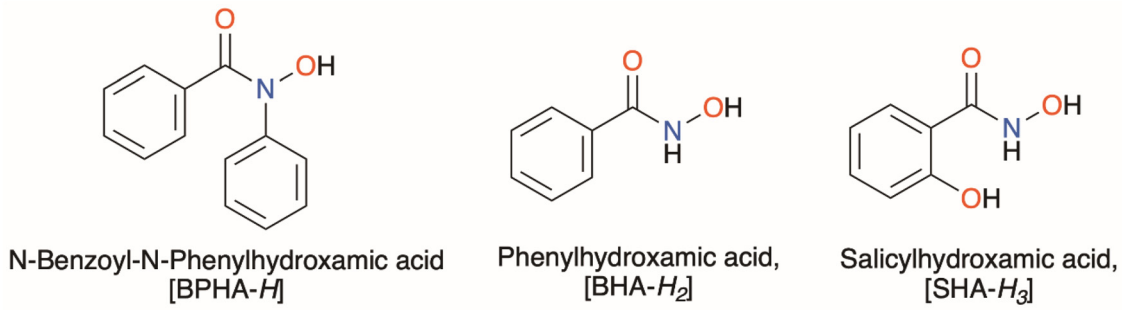

Fig. 1 The three hydroxamic acids used in this study: BPHA-*H* = *N*-benzoyl-*N*-phenylhydroxamic acid, BHA-H_2 = phenylhydroxamic acid, and SHA-H_3 = salicylhydroxamic acid.

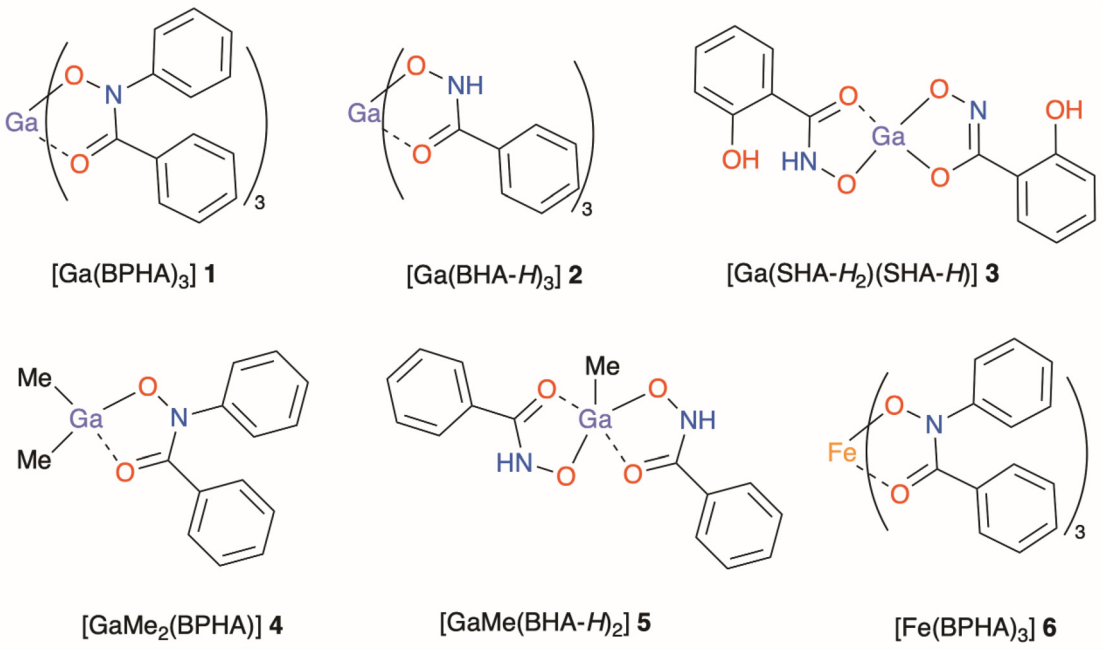

Fig. 2 Complexes synthesised in this study: [Ga(BPHA$_3$)] **1**, [Ga(BHA-*H*)$_3$] **2**, and [Ga(SHA-*H*$_2$)(SHA-*H*)] **3**, [GaMe$_2$(BPHA)] **4**, [GaMe(BHA-*H*)$_2$] **5** and [Fe(BPHA)$_3$] **6**.

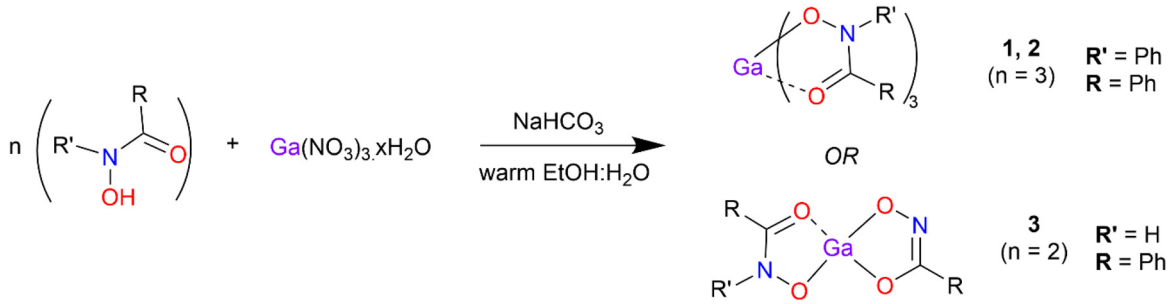

Scheme 1 Synthetic pathway for synthesis of the gallium hydroxamate/hydroximate complexes **1** and **2** and **3**.

Results and discussion

Synthesis and characterisation

Gallium complexes [Ga(BPHA)$_3$] **1**, [Ga(BHA-*H*)$_3$] **2**, and [Ga(SHA-*H*$_2$)(SHA-*H*)] **3**, were synthesised (Scheme 1) through the solid addition of the gallium nitrate to a 1 : 1 ethanol : water solution of the hydroxamic acid heated to 60 °C. $NaHCO_3$ was then added to bring the solution pH up to *ca.* 7 at which point the metal complex precipitated. The products, as white to off-white powders, were collected *via* gravity filtration and washed with copious amounts of water before air drying.

The organometallic heteroleptic complexes [GaMe$_2$(BPHA)] **4** and [GaMe(BHA-*H*)$_2$] **5** were synthesised through the direct addition of neat trimethyl gallium to a suspension of the pre-dried hydroxamic acid under inert conditions in dry hexane at 0 °C (Scheme 2). Despite multiple attempts to synthesise and isolate the dimethyl gallium benzohydroxamate complex, [GaMe$_2$(BHA-*H*)], the reaction would rapidly proceed to the formation of the mono-methyl bis-hydroxamate complex **5**, [GaMe(BHA-*H*)$_2$]. To maximise the yield of **5**, the required 2 : 1 reaction stoichiometry was used. For complex **4**, the opposite was observed wherein attempted formation and isolation of a bis-hydroxamate complex, [GaMe(BPHA)$_2$], would invariably result in isolation of the dimethyl mono-hydroxamate complex **4**. Attempts to synthesise an organogallium complex derived from SHA-H_3 consistently resulted in the formation of multiple products and a pure isolable complex could not be obtained. Since the biological assays require complex purity, this reaction was not studied further at this time.

These gallium complexes were all characterised through ^{1}H and ^{13}C NMR spectroscopy, FT-IR spectroscopy, ESI-mass spectrometry, elemental analysis, melting point analysis, and where applicable single crystal X-ray diffraction.

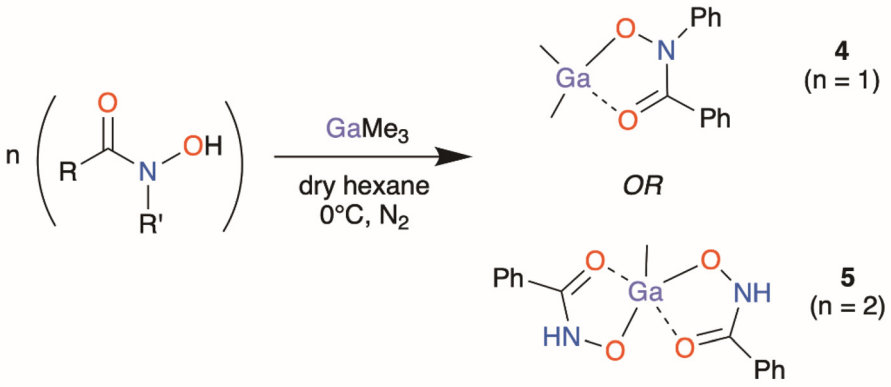

Scheme 2 Synthetic pathway for the acquisition of the organometallic gallium complexes **4** and **5**.

During the attempted syntheses of these complexes, several crystalline products were obtained in low yield which were indicative of the impact of solvent, ligand redistribution and hydrolysis on the reaction mixtures and products. These were; the heteroleptic methanolysis product [Ga(BPHA)$_2$(OMe)] **7**, the tetra-nuclear oxido cluster [Ga$_4$Me$_7$(BPHA)O$_4$] **8**, the mono-methyl complex [GaMe(BPHA)$_2$] **9**, and [{GaMe$_2$(BHA-*H*)}{Ga$_2$Me$_4$O}], **10**. A summary of the conditions under which these complexes were obtained, their X-ray data, and any further analysis is provided in the ESI.†

Understanding that there is always the potential for exchange of gallium for iron in biological media (and also *in vivo*) the iron complex [Fe(BPHA)$_3$] **6**, being the analogue of **1**, was synthesised from the reaction of FeCl$_3$ with BPHA-*H* (Scheme 3). This was able to be crystallised and the solid-state structure determined. It was further characterised by ESI-MS, FT-IR, and elemental analysis.

X-ray crystallography

Single crystals of complexes **1**, **4**, **5** and **6** were obtained through slow evaporation in solvent. The additional solid-state structures for **7**, **8** and **10** are given in the ESI (Fig. S12–S15†). The tris-hydroxamato complexes [Ga(BPHA)$_3$] **1** and [Fe(BPHA)$_3$] **6** crystallise with high symmetry, and with a distorted octahedral coordination environment, Fig. 3. A detailed summary of bond lengths and angles for the solid-state structures of these complexes are given in in the ESI (Table S1†). Due to the high symmetry of **1**, and axial rotation of the ligands, the carbon and nitrogen atoms in the 'O–C–N–O' backbone of BPHA are superimposed and so were modelled over the two positions. The degree of distortion away from an ideal octahedron was found to be greater for iron than gallium, with the iron complex exhibiting an angle of 98.17(14) through the O(1A)–Fe–O(1B) bond.

Crystals of complexes **4** and **5** were obtained through slow evaporation in toluene. The coordination environments and geometries for complexes [GaMe$_2$(BPHA)] **4** and [GaMe$_2$(BPHA)] **5** were found to be similar to the those we recently reported for di-methyl and mono-methyl gallium quinolinolato complexes. As shown in Fig. 4, complex **4** is four coordinate with a typical tetrahedral geometry, while **5** is five coordinate and trigonal bipyramidal.[22]

As evidenced by the bond lengths, and illustrated in Fig. 2, the mono-anionic hydroxamate ligands in complexes **1**, **4**, **5** and **6** all show a similar bonding {O=C(–R)–N–O$^-$} pattern for the metal chelating moiety.

FT-IR data correlates well with the hydroxamate ligand conformation observed in complexes **1**, **4**, **5** and **6** (ESI†). In all complexes, the typical broad O–H stretch at *ca.* ~3100 cm^{-1} found in the spectrum of each of the hydroxamic acids is absent in the spectrum of each of the corresponding complexes. Supporting this, Table 1 provides the carbonyl absorbances and amide absorbances for each of the gallium complexes and the subsequent shift to lower wavenumbers of the corresponding symmetric and asymmetric stretches in the metal complexes, evidence of mono-anion formation, metal complexation, and chelation.

For complex **2**, complexation of the hydroxamate ligand was identified by the significant shift in the carbonyl stretches from 1622 cm^{-1} to 1598 cm^{-1} similar to that observed for **1**. Supporting this, a weak N–H stretch is observed at 3356 cm^{-1} which is blue-shifted compared to the strong N–H stretching signal 3286 cm^{-1} for the hydroxamic acid.

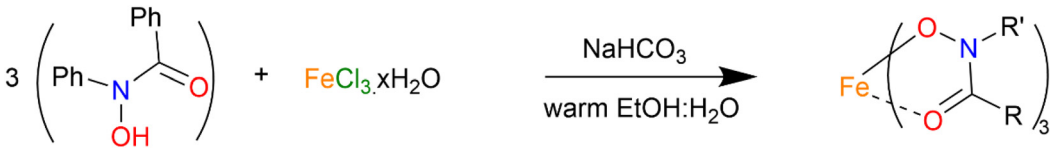

Scheme 3 Synthetic pathway for the formation of complex [Fe(BPHA)$_3$] **6**.

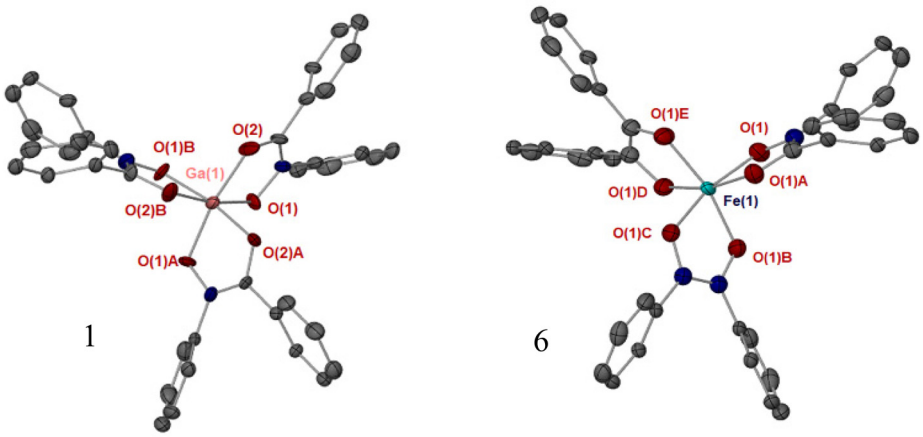

Fig. 3 Solid-state structures of complexes [Ga(BPHA)$_3$] **1** and [Fe(BPHA)$_3$] **6**. Thermal ellipsoids at 50% probability, hydrogen atoms have been omitted for clarity. Symmetry operators: **1**, $(1 - X + Y, 1 - X, Z) : (1 - Y, X - Y, Z)$; **6** $(Y, X, \frac{1}{2} - Z) : (-Y, X - Y, Z) : (-X, -X + Y, \frac{1}{2} - Z) : (-X + Y, -X, Z) : (X - Y, -Y, \frac{1}{2} - Z)$. Selected bond length (Å) **1**: Ga(1)–O(1), 1.972(2), O(1)–N(1), 1.389(12), O(1)–C(2), 1.257(28). **6**: Fe(1)–O(1), 2.001(3), O(2)–C(1): 1.322(5) Angles (°) G1: O(1)–Ga(1)–O(2), 91.64(8), O(1)–Ga(1)–O(1B), 169.6(1). **6**: O(1)–Fe(1)–O(2), 92.45(12), O(1)–Fe(1)–O(1B), 166.1(2).

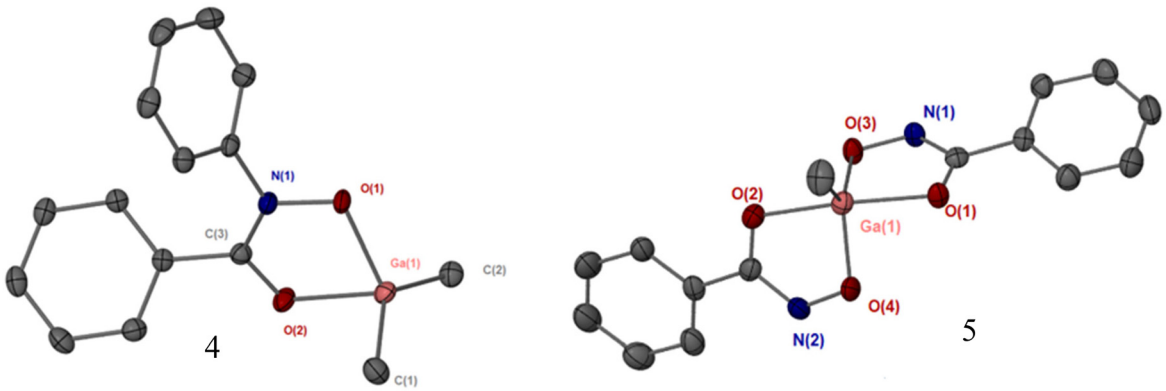

Fig. 4 Crystal structures of complex **4**, [GaMe$_2$(BPHA)] and complex **5**, [GaMe(BHA-*H*)$_2$] (note: interstitial toluene molecule in **5** excluded for clarity). Thermal ellipsoids at 50%, hydrogen atoms omitted for clarity. Selected bond lengths (Å) and angles (°): **4**, [GaMe$_2$(BPHA)]: Ga(1)–O(1), 1.958(1), Ga(1)–O(1′), 2.544(1), Ga(1)–O(2), 2.062(1), Ga(1)–C(1), 1.949(2), Ga(1)–C(2), 1.951(2). O(1)–Ga(1)–O(1′) 68.86(5), O(1)–Ga(1)–O(2) 79.47(5), O(2)–Ga(1)–O(1′), 147.6(1), C(1)–Ga(1)–O(1), 113.4(1), C(2)–Ga(1)–O(1) 110.0(1). **5**, [GaMe(BHA-*H*)$_2$]: Ga(1)–O(1), 2.040(2), Ga(1)–O(2), 2.067(2), Ga(1)–O(3), 1.906(2), Ga(1)–O(4), 1.902(2), Ga(1)–C(1), 1.935(2). O(1)–Ga(1)–O(2), 157.8(1), O(1)–Ga(1)–O(3) 82.18(6), O(1)–Ga(1)–O(4), 89.28(7), O(3)–Ga(1)–O(4), 108.2(1), C(1)–Ga(1)–O(1), 101.8(1), C(1)–Ga(1)–O(3).

Table 1 FT-IR absorbance frequencies of gallium complexes **1–5**

	IR absorbance (cm^{-1})				
Complex	C═O$_{sym}$	C═O$_{asym}$	N–H	C═N	C–H
1 [Ga(BPHA)$_3$]	1582	1517	3050	—	—
2 [Ga(BHA-*H*)$_3$]	1598	1517	3356	—	—
3 [Ga(SHA-*H*$_2$)(SHA-*H*)$_3$]	1574	1516	—	1601	—
4 [GaMe$_2$(BPHA)]	1586	1535	3060	—	2961
5 [GaMe(BHA-*H*)$_2$]	1601	1534	3194	—	3007

In contrast, the FT-IR spectrum of **3** coupled with elemental analysis data indicates that the solid-state structure of this complex is heteroleptic, composed of a hydroxamate (SHA-*H*$_2$) and hydroximate (SHA-*H*) ligand chelating into the Ga centre, [Ga(SHA-*H*$_2$)(SHA-*H*)]. Thermogravimetric analysis (TGA) suggests the presence of one moiety of water per compound (ESI Fig. S2†). The absence of the N–H stretch at 3285 cm^{-1} suggested deprotonation of the imine functional group. Furthermore, the additional large hydroxyl signal of the phenol further masks the N–H absorbance. The strong C═N band at 1601 cm^{-1}, absent in the FTIR spectra for other five complexes, alludes to the presence of the hydroximate ligand.

For complexes **1** and **2** the hydroxamate form was observed in the NMR spectra (see ESI†). The predominant form in the solid state for complexes **2** and **3** was confirmed by elemental analysis to be the hydroxamate–hydroximate bis-hydroxamate substitution, with solution state data highlighting a shift to a tris-substituted hydroxamate state (Fig. S1†). Thermogravimetric analysis (TGA) revealed that complexes **2** and **3** were hygroscopic with a loss of 3.8567% and 3.0727%

mass respectively at 100 °C, equivalent to one H_2O molecule for one molecule of **2** and one H_2O for two **3** molecules, as confirmed *via* elemental microanalysis (Fig. S2 and S4†). Complex **1** was observed to be the tris-hydroxamate in both the solution and solid-states, supported by the X-ray data. For the alkyl analogues **4**, and **5** only the hydroxamate form was observed as confirmed by XRD analysis, showing the carbonyl oxygen providing a dative interaction and stabilising the complex through chelation of the ligand. The absence of the hydroxyl proton of the free acids in the NMR spectrum provided further evidence of deprotonation and metal-chelation. Shifts were observed in the aromatic regions of the free acids *versus* the complexes. An example spectrum of complex **1**, **4** and free BPHAH can be found in the ESI.†

Changes in complex composition in the solid-state *versus* solution state was also able to be confirmed with ESI-MS. For **3**, both ([Ga(SHA-H_2)(SHA-H)] + Na^+, 395.0)$^+$ and ([Ga(SHA-H_2)$_3$] + Na^+, 548.0)$^+$ were observed.

Biological testing

Stability studies and water solubility. Prior to *in vitro* bioassays, the gallium complexes **1–5** were studied for their stability in both solid and solution states, particularly their sensitivity towards hydrolysis. Repeated melting point analysis over a period of three months showed no compositional change in the complexes. No changes were observed in the NMR spectra of the complexes in DMSO-d_6 taken over a period of 24 hours indicating stability towards hydrolysis. Aqueous solubility can play a role in the activity of metallodrugs. Complexes of higher lipophilicity are more likely to traverse cellular membranes.[23] ICP-MS/OES was used to determine the solubility (details in the Experimental section, calibration curves in ESI, Fig. S5†). Corresponding values are given in Table 2. Unsurprisingly, **1** was the least water-soluble of the tris-hydroxamato complexes (4.90 μg mL^{-1}), with **2** exhibiting the highest degree of water solubility (41.84 μg mL^{-1}). Both alkyl complexes, **4** and **5**, exhibited the lowest degree of water solubility, reflecting the greater lipophilicity of the Me ligands.

Mammalian viability assays. Ideally, the gallium complexes **1–5** show low systemic toxicity toward mammalian cell lines allowing for selectivity towards the bacterial cells. To assess this a simple cell viability assay utilising the fluorescent resazurin–resorufin metabolic reduction was conducted,[24] employing L929 primary mouse fibroblast cells. Complexes were dissolved into DMSO at a working stock of 10 mM before addition to the well plate. The free hydroxamic acids, metal nitrate, the iron complex **6** and DMSO were all used as controls (ESI, Fig. S6†). These controls showed no changes to cell viability over a 24 hours period (see ESI†). Complexes **2**, **3**, **4** and **5** exhibited no degree of cell inhibition, with IC_{50} values ≥100 μM. **1** exhibited the highest degrees of inhibition with an IC_{50} value of 67.3 μM (Table 3 and Fig. S7†). This may be associated with the lower aqueous solubility and hence greater lipophilicity of the complex. Increased lipophilicity, which improves cellular uptake, is known to be reflected in increased host cell toxicity.[23] Even at this level, these values are still significantly low when compared to some TGA and FDA approved metal-based therapeutics, for example cisplatin.[25,26]

Minimum inhibitory concentrations (MICs). With little to no mammalian cell toxicity observed for the complexes, their anti-bacterial activity in both an iron rich media (LB-broth) and an iron poor media (RPMI-HS) was assessed.

LB media. The gallium complexes **1–5**, along with the metal nitrates and the free hydroxamic acids, were all assayed in triplicate against a range of bacteria; MRSA, VRE, *E. coli*, *A. baumannii*, *P. aeruginosa*, and *K. pneumoniae.* Graphs showing MIC values are available in the ESI, Fig. S8.† None of the complexes showed activity towards the Gram-positive strains and *E. coli* in the iron-rich LB-broth (Table 4). The alkyl gallium complexes, **4** and **5**, exhibited activity at the highest concentration (100 μM) toward the Gram-negative bacteria *K. pneumoniae*, *A. baumannii* and *P. aeruginosa*, with all tris-hydroxamate complexes showing no observable activity (Table 4 and Fig. S9†).

RPMI-HS media. Analysis of the five Ga complexes in iron-poor RPMI-HS media showed no activity towards the Gram-negative bacterial strains for the metal–organic complexes **1–3**, similar for the assays in iron rich LB media. However, the alkyl complexes **4** and **5** showed drastically enhanced activity and selectivity for the multi-drug resistant (MDR) strain of *K. pneumoniae* (KP1074) with complete inhibition of growth at concentrations as low as 78.0 nM (Table 5 and Fig. S10†). Interestingly, no activity was observed towards *A. baumannii* or *P. aeruginosa* indicating a unique mode of action for the organogallium complexes towards *K. pneumoniae.* A study in 2017 found the thiosemicarbazone Ga(III) complex [Ga($C_{14}H_{14}N_4S$)$_2$$NO_3$·$2H_2O$] active toward a broad spectrum of both Gram positive and Gram negative bacteria. It is interesting to note the selective difference between an inorganic complex and the organogallium compounds in this study.[27]

Table 2 Solubility of the gallium complexes in water determined *via* ICP-MS. All analyses were completed in triplicate

Complex	Aqueous solubility (μg mL^{-1})
1 [Ga(BPHA)$_3$]	4.90
2 [Ga(BHA-H)$_3$]	41.8
3 [Ga(SHA-H_2)(SHA-H)$_3$]	33.6
4 [GaMe$_2$(BPHA)]	0.989
5 [GaMe(BHA-H)$_2$]	0.851

Table 3 IC_{50} values determined spectroscopically toward mammalian control cell L292 mice fibroblasts. All analyses were conducted in triplicate

Complex	IC_{50} (μM)
1 [Ga(BPHA)$_3$]	67.3
2 [Ga(BHA-H)$_3$]	>100
3 [Ga(SHA-H_2)(SHA-H)$_3$]	>100
4 [GaMe$_2$(BPHA)]	>100
5 [GaMe(BHA-H)$_2$]	>100
6 [Fe(BPHA)$_3$]	>100

Table 4 MIC (μM) values of complexes **1–6** toward bacteria in iron rich LB-broth. All analyses were conducted in triplicate. PA = *P. aeruginosa*, AB = *A. baumannii*, KP = *K. pneumoniae*, KP1074 = MDR *K. pneumoniae* 1074, VRE = vancomycin resistant *Enterococcus*, EC = *E. coli*, MRSA = methicillin resistant *S. aureus*

	MIC (μM)						
Complex	PA	AB	KP	KP1074	EC	VRE	MRSA
1 [Ga(BPHA)$_3$]	≥100	≥100	≥100	≥100	≥100	≥100	≥100
2 [Ga(BHA-*H*)$_3$]	≥100	≥100	≥100	≥100	≥100	≥100	≥100
3 [Ga(SHA-H_2)(SHA-*H*)$_3$]	≥100	≥100	≥100	≥100	≥100	≥100	≥100
4 [GaMe$_2$(BPHA)]	100	100	100	100	≥100	≥100	≥100
5 [GaMe(BHA-*H*)$_2$]	100	100	100	100	≥100	≥100	≥100
6 [Fe(BPHA)$_3$]	—	—	≥100	≥100	—	—	—

Table 5 MIC (μM) values of complexes **1–6** toward Gram negative bacteria *P. aeruginosa*, *A. baumannii* and MDR *K. pneumoniae* (KP1074) in RPMI-HS. All analyses were conducted in triplicate

	MIC (μM)		
Complex	PA	AB	KP1074
1 [Ga(BPHA)$_3$]	≥100	≥100	≥100
2 [Ga(BHA-*H*)$_3$]	≥100	≥100	≥100
3 [Ga(SHA-H_2)(SHA-*H*)$_3$]	≥100	≥100	≥100
4 [GaMe$_2$(BPHA)]	100	100	**0.078**
5 [GaMe(BHA-*H*)$_2$]	100	100	**0.078**
6 [Fe(BPHA)$_3$]	—	—	≥100
[GaMe$_2$(OH)]	—	—	**0.156**

As we have observed before, the controls for the reference strain of *K. pneumoniae* did not show significant growth in RPMI-HS, and hence no MIC was obtainable, and we believe is most likely due to the presence of antimicrobial peptides found in human serum.[20,21] Furthermore, the presence of the MagA gene in MDR *K. pneumoniae*, which up-regulates the production of hypermucoviscosity, is said to demonstrate an extraordinarily high resistance to the antimicrobial properties of complement-human serum.[28]

With the increased activity toward KP1074 obtained, controls were then assessed to determine whether the complex itself exudes the activity. The free acids BHA-H_2 and BPHA-*H* were analysed for their inhibitory activity at the same concentration as the complexes. The iron complex [Fe(BPHA)$_3$] **6** and the potential hydrolysis product [GaMe$_2$OH] were also analysed at the same concentration gradient. Unsurprisingly, the tris-hydroxamato Fe complex and the free acids exhibited no activity in RPMI-HS, however [GaMe$_2$OH] exhibited activity comparable to complexes **4** and **5** with an MIC of 156.0 nM.

While this is significant, **4** and **5** still have activity two-fold higher indicating that the hydroxamate ligands are important in the overall antibacterial activity but that the 'GaMe$_2$' and 'GaMe' moieties are critical in their effect on MDR *K. pneumoniae* (see ESI† for example inhibition images).

The effect of iron. Recent studies into the antimicrobial activity of gallium have found that simple salts such as gallium nitrate (GaN) and gallium citrate (GaCi) can exhibit enhanced activity toward resistant nosocomial pathogens in the iron-poor assay environment provided by RPMI media supplemented with human serum.[29] Importantly, these salts are highly water soluble and labile thus making Ga highly bioavailable and rapidly transfer Ga to plasma proteins which differs greatly to the complexes in this study. The lack of activity from **1** and **2** was surprising given they are *O'O* chelated homoleptic tris-substituted complexes similar to gallium maltolate (GaM).

GaM has been shown to have a high bioavailability due to the prolonged absorption into the blood stream, allowing uptake of the Ga^{3+} ions by transferrin as opposed to rapid formation of gallate $[Ga(OH)_4]^-$.[30,31] It is possible that complexes **1** and **2** are rapidly hydrolysed in aqueous media, leading to gallate formation, possibly rapidly exchange with iron (discussed further), and/or undergo rapid ligand exchange with transferrin or lactoferrin, thereby preventing uptake by the bacteria that rely less on methods of host-peptide iron sequestration. In contrast, the alkyl complexes may provide a greater degree of hydrolytic stability given the relatively inert nature of the remaining Ga–Me bonds. A study by Coggin *et al.* in the early 90s detailed the hydrolytic stability of the Ga–C bond in four-coordinate gallium complexes and determined with *in vivo* rat studies that protein adducts of $[GaMe_2]^+$ are either kinetically labile or not formed.[32] Recently, we determined that complexation may play a role in potential iron exchange processes in iron-depleted media. Our analysis of both organo gallium quinolonates and quinolinolates showcased a lower degree of protein association in RPMI-HS than their homoleptic analgoues.[20,21] Therefore, we investigated whether this property would translate to the siderophore mimicking hydroxamates. To allow for direct comparison in this experiment, only hydroxamate bearing complexes derived from BHA-H_2 and BPHA-*H* were explored, thus excluding complex **3**. However, because of its significant activity [GaMe$_2$(OH)] was examined. Triplicate gallium analysis of both the digested extracted protein pellet phase and aqueous supernatant by ICP-MS supported the hypothesis that the metal–organic complexes **1** and **2** are rapidly hydrolysed and/or exchanged with iron into mammalian iron sequestering proteins,

whereas the increased hydrolytic stability of the alkyl gallium complexes **4**, **5** and [$GaMe_2$(OH)] does not allow free access to Ga^{3+} ions in solution, leading to decreased uptake by transferrin and/or lactoferrin (Table 6 and Fig. S11†). Additionally, this uptake is supported further by the similar levels of Ga observed for [$GaMe_2$(OH)] (Table 6). As previously mentioned, in iron poor conditions *K. pneumoniae* will up-regulate the production of siderophores in order to maximise its ability to scavenge iron.[12] These combined factors may provide the basis for the increased activity of complexes **4** and **5** and [$GaMe_2$(OH)] toward *K. pneumoniae* in RPMI-HS.

Gallium–iron exchange. To understand the possible rapid exchange of the homoleptic complexes with iron, a solution of complex **1** [$Ga(BPHA)_3$], as an exemplar, was titrated with aliquots of $FeCl_3$ and monitored by UV-visible spectrophotometry. A decrease in the absorption maxima of **1** of 284 nm was apparent with each addition, with the three previously determined absorption maxima of **6** (225, 276 and 422 nm) becoming more prominent (Fig. 5). A clear change from colourless to red in acetonitrile was observed with the dissociation of gallium from the hydroxamate complex, and substitution of iron. From titrating a 10 μM solution of **1** with 3 mL of a 10 μM solution of $FeCl_3$ a concentration of 6.91 μM of **6** was generated. Therefore, it can be concluded that a rapid exchange process is occurring. Though favourable in some bacterial species in which heme and other mammalian proteins are the major source of exogenous iron, this exchange process would be unfavourable in mammalian cells. This exchange may potentially occur with iron rich proteins such as transferrin, which has proven to have a higher affinity for gallium than iron.[33–36] However, this study was concluded with gallium salts such as gallium nitrate and gallium citrate.[17,33] More thermodynamically stable and kinetically inert complexes such as gallium maltolate and gallium tris-quinolinolate either exhibited a much slower rate of transfer, or no transfer at all.[3] This would indicate that ligand class and coordination geometry of the gallium plays a vital role in its ability to exchange with iron proteins.

Table 6 Gallium content in supernatant (RPMI + acetonitrile) *versus* protein pellet at times points initial and 24 hours. Gallium content measured *via* ICP-MS. All analyses were conducted in triplicate

Complex	Supernatant initial (%)	Pellet initial (%)	Supernatant 24 h (%)	Pellet 24 h (%)
1 [$Ga(BPHA)_3$]	19.9 + 7.27	80.1 + 12.6	16.2 + 2.04	83.8 + 8.37
2 [$Ga(BHA\text{-}H)_3$]	16.4 + 8.95	83.6 + 5.75	19.0 + 7.10	81.0 + 18.0
4 [$GaMe_2$(BPHA)]	72.4 + 1.95	27.6 + 4.69	20.1 + 6.44	79.9 + 18.2
5 [GaMe(BHA-*H*)$_2$]	83.5 + 8.95	16.5 + 0.945	23.3 + 4.60	76.7 + 19.3
[$GaMe_2$(OH)]	78.2 + 4.21	21.8 + 1.22	36.0 + 2.94	64.0 + 12.04

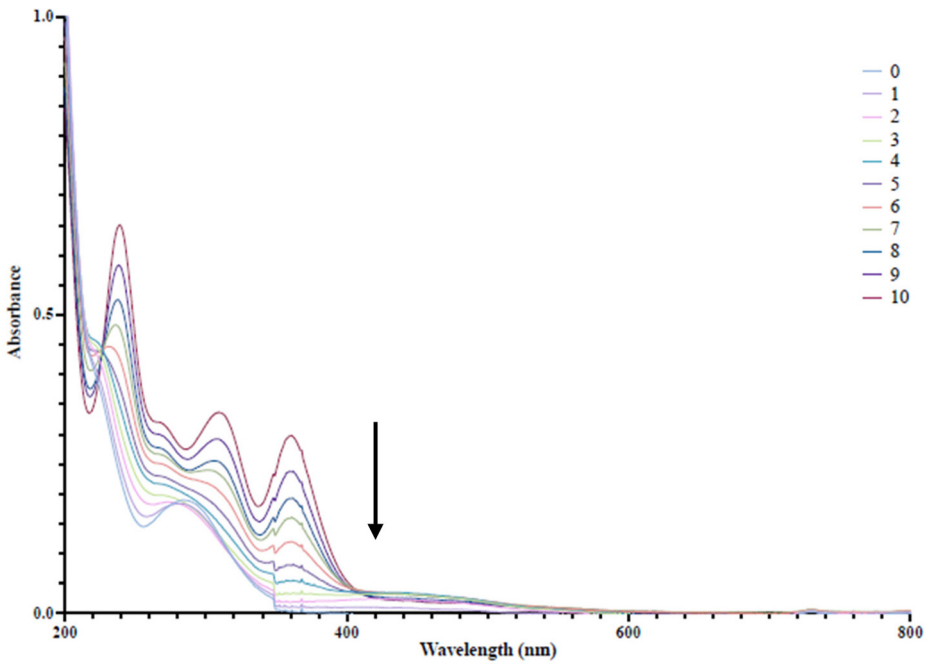

Fig. 5 UV-visible spectra of aliquots taken after 1 mL addition of 10 μM $FeCl_3$ used to determine the 'end-point' of titration.

Conclusions

Five gallium complexes; three metal–organic [Ga(BPHA)$_3$] **1**, [Ga(BHA-*H*)$_3$] **2**, [Ga(SHA-*H*$_2$)(SHA-*H*)] **3**, and two heteroleptic organometallic [GaMe$_2$(BPHA)] **4**, [GaMe(BHA-*H*)$_2$] **5**, and the iron complex [Fe(BPHA)$_3$] **6**, were synthesised and fully characterised. Complex **3** was found to adopt a mixed ligand hydroximate–hydroxamate composition [Ga(SHA-*H*$_2$)(SHA-*H*)] in the solid state which in solution exists in an equilibrium mixture with the homoleptic tris-hydroxamato complex [Ga(SHA-*H*)$_3$]. The complexes were found to be stable to air and moisture in the solid-state over a period of three months. Single crystal XRD studies confirmed that **1** and **6** adopted analogous O′O chelating six coordinate environments at the metal centres, though the Fe complex shows greater distortion from ideal octahedral coordination than the Ga complex. Complex **4** presented as four-coordinate tetrahedral while **5** presented as trigonal bipyramidal with a 5-coordinate centre.

These complexes were tested for their anti-microbial activity and mammalian cell viability. Only **1** exhibited any degree of mammalian cell inhibition, with an IC_{50} value of 67.3 μM. The other four complexes were found to be non-toxic towards L929 mouse fibroblast cells at 100 μM, the highest concentration tested.

The anti-bacterial activity of the complexes is dependent on the media in which the assays were conducted. In the iron supplement LB media, no activity was observed towards either of the Gram-positive strains of MRSA or VRE. However, some activity was seen towards the three Gram-negative strains of *P. aeruginosa*, *A. baumannii*, and *K. pneumoniae*, with all showing MIC values of 100 μM.

Analysis in the low iron, and more physiologically relevant, RPMI-HS media showed a drastic increase in the antibacterial activity of complexes **4** and **5** toward *K. pneumoniae*, with MIC values as low as 78.0 nM. No change in activity was observed for the metal–organic complexes **1** and **2**. This radical difference in activity may be due in part to the increased hydrolytic stability of the methyl gallium (Ga–C) bonds and the propensity for the metal–organic gallium complexes to readily exchange with iron, as demonstrated by both the protein uptake analysis and UV-Vis titration study.

With nanomolar *in vitro* activity, the methyl gallium hydroxamate complexes **4** and **5** provide for a new and promising class of gallium-based therapeutics for challenging *K. pneumoniae* infections and biofilms.

Experimental section

General

Reagents were purchased from Sigma Aldrich, Merck, Otsuka Pharmaceuticals and Thermo Fisher without the need for further purification. Solvents were purchased from Merck and where required dried using an MBRUAN SPS-800 solvent purification system and stored over 4 Å molecular sieves. All reaction requiring inert conditions were performed under an atmosphere of nitrogen, using oven dried glassware and utilising a Schlenk manifold and technique. ^{1}H NMR and ^{13}C NMR were recorded on a Bruker Ultrashield Plus 600 DRX600 spectrophotometer (600 MHz), chemical shifts were referenced to the appropriate solvent, DMSO-d$_6$. Variable temperature NMR was recorded on a Bruker Avance DRX400 spectrophotometer (400 MHz) Melting point analysis was conducted in open end capillary tubes, on a digital Stuart Scientific melting point apparatus SMP10. Infrared Spectra were recorded on an Agilent Technologies Cary 630 FTIR spectrometer, using a range of 4000–500 cm^{-1}. Mass spectrometry (ESI) was obtained utilising a Micromass Platform QMS spectrometer, with an electrospray source and a cone voltage of 35 eV. Elemental analysis was obtained from the School of Chemistry, Monash University. Solubility of complexes in H_2O was determined using inductively coupled plasma mass spectrometry (ICP-MS) on a PerkinElmer NexION 2000 ICP-MS instrument. An internal standard of 20 ppb Ag/As in 2–3% HNO_3 was used and 11-point calibration curves of gallium and indium were generated. Samples were prepared by adding compound 100 μL of H_2O, vortexing for 30 s to ensure the point of saturation has been reached. These samples were left to incubate overnight at room temperature before being centrifuged at 3000 rpm for 5 min and a 10 μL aliquot of solution was diluted to 10 mL using 2–3% HNO_3. All volumes were determined by weight and the dilution factor was used to calculate the final solubility value. Ultraviolet–visible spectra were recorded on an Agilent Technologies Cary 100 UV-visible spectrometer in the range of 200 to 800 nm. Absorbance readings were conducted in 10 mm innovative Lab Supply ES Quartz cuvettes using acetonitrile as a solvent. Blank measurements were conducted using acetonitrile. Thermogravimetric analysis (TGA) was carried out using a Mettler Toledo TGA/DSC 1 Star System with heating up to 400 °C.

X-ray crystallography

Crystallographic data was collected on an OXFORD XtaLAB Synergy, Dualflex, HyPix diffractometer equipped with an OXFORD Cryosystems 700 Cryostream and cooled to 173(2) K. Each compound was solved and refined using SHELXL-2014/7 utilising the graphical interface X-Seed or Olex2.[37,38] Unless otherwise indicated, all non-hydrogen atoms were refined with anisotropic thermal parameters. Hydrogen atoms were placed in calculated positions using a riding model with C–H = 0.95–0.98 Å and U_{iso}(H) = xU_{iso}(C), x = 1.2 or 1.5 unless otherwise indicated.

Biological testing

Human serum (H4522), Fetal Bovine Serum (FBS), Dulbecco's modified Eagle's medium, penicillin–streptomycin solution (pen–strep), and GlutaMAX™ Supplement was purchased from Gibco/Thermo-Fisher. RPMI-1640 medium was purchased from the Biomedicine Discovery Institute, Monash University. Mouse fibroblasts; NCTC clone 929 [L cell, L-929, derivative of Strain L] (ATCC CCL-1).

Bacteria preparation and MICs. MRSA (M118797, methicillin-resistant *Staphylococcus aureus*), VRE (M846910, vancomycin-resistant *Enterococcus faecalis*) *Escherichia coli* (102), *Psuedomonas aeruginosa* (ATCC27853) and *Acinetobacter baumannii* (C403/ATCC17978) were grown in LB (Luria–Bertani) broth. Bacteria from glycerol stocks were streaked onto Nutrient or LB agar and incubated overnight at 37 °C and subsequently a single colony was inoculated into 3 mL of BHI or LB broth and incubated for 18 to 20 hours at 37 °C and 180 rpm to give turbid overnight cultures. Stock solutions were generated by solubilising **1**, and $[Ga(NO_3)_3{\cdot}9H_2O]$ in DMSO at 10 mM. Stock solutions were generated by solubilising **2**, **3**, **4**, **5**, [BPHA-H_2], [BHA-H_2], and [SHA-H_3] in DMSO at 20 mM. The stocks were first diluted in sterile water, then in BHI or LB broth in 96-well plates, to give a maximum concentration of 100 μM (excluding MeOH, which had a maximum concentration of 50 μM). This was serially diluted by a factor of two with a total of 100 μL per well. Overnight bacterial cultures were diluted to approximately 10^4 colony forming units per mL in BHI, LB broth or RPMI-HS, before addition of 5 μL to each well and incubation at 37 °C for 20 to 22 hours. MICs were defined as the point in which no visual growth was observed. All analyses were done in triplicate. A separate analysis was prepared for KP1074 and complexes **4**, **5** and $[GaMe_2(OH)]$. Briefly: bacteria were grown as per the previous procedure and an inoculum obtained. In 15 mL falcon tubes, a dilution gradient of the compounds from 100 μM–0.39 μM was obtained in 1 mL total volume. To this, 50 μL of diluted bacteria inoculum was added. These were incubated as previous. The MIC was defined as the point at which no visual growth was observed.

Cell culture. L929 fibroblasts were cultured and maintained in Dulbecco's Modified Eagle Medium (DMEM) supplemented with 10% Fetal Bovine Serum (FBS), 1% Pen–Strep and 1% GlutaMAX™ at 37 °C in a 5% CO_2 incubator.[39–42]

***In vitro* testing of L929 cells.** Resazurin was used for the determination of the percentage viability of L929 fibroblast cells. Working stock solutions were generated by solubilising, $Ga(NO_3)_3{\cdot}9H_2O$, $In(NO_3)_3{\cdot}3H_2O$, MeOH, **1**, **2**, **3**, **4**, **5**, [BPHA-H_2], [BHA-H_2], and [SHA-H_3] in DMSO at 10 mM. Stock solutions were then sequentially diluted out in the appropriate culture media to give a maximum concentration of 100 μM (excluding MeOH, which had a maximum concentration of 50 μM). Volumes of 10^5 L929 per mL were seeded and adhered to 96-well plates 24 hours prior to compound addition. 20 hours after compound addition, 20 μL of resazurin in PBS was added to each well, then incubated for a further 4 hours. All cell assays were measured spectroscopically using fluorescence excitation at 560 nm and emission at 590 nm. The compounds were compared to a positive control of no compound and the percent inhibition was calculated.[43] Fluorescence measurements were conducted using a Thermo Scientific Varioskan LUX Multimode Microplate Reader (shaking: 15 s, 300 rpm, high force, single orbital). Experiments were conducted independently in triplicate, with values averaged between the experiments. IC_{50} values were determined using GraphPad Prism 9.[44]

Protein binding analysis. 20 mM stocks of complexes **1**, **2**, **4**, **5** and $[GaMe_2(OH)]$ were made up in biological grade DMSO to a volume of 1 mL. From these stocks, an aliquot of 10 μL were added to 990 μL of RPMI-1640 + 10% human serum to give a total complex concentration of 200 μM per sample. The solutions were vortexed vigorously. 24-hour samples were incubated at 37 °C overnight with shaking. Samples were taken at time point "zero" and 24 h. At the set time point (zero or 24 hours) 1000 μL of acetonitrile was added to the samples to extract all proteins through precipitation. The samples were then centrifuged to pellet the precipitates and the supernatant (RPMI + acetonitrile) separated. The protein pellet was digested with 70% nitric acid though gentle heating and sonication. Both the supernatant and acid digested pellet were then diluted to a final volume of 5 mL in separate 15 mL falcon tubes with 2–3% nitric acid in ultrapure water. Prior to analysis, pellet samples were filtered through a 0.23-micron filter tip into a fresh tube to remove any trace particulates. Samples were then analysed on a PerkinElmer NexIon ICP-MS against a 10-point calibration curve. The gallium content in each phase was obtained and then compared to the total gallium in each sample (precipitate + supernatant) as a percentage of gallium per phase. All analyses were done in triplicate.

General procedures

Caution: $GaMe_3$ is a pyrophoric liquid and can ignite on contact with air and moisture. It should always be handled carefully under inert atmosphere conditions with appropriate glassware and equipment.

Synthesis of dimethyl gallium hydroxide, $[GaMe_2(OH)]$. Gallium trichloride (1 mmol 0.194 g) was weighed into a Schlenk and dissolved into 20 mL of pre-dried diethyl ether. The solution was cooled to −78 °C before dropwise addition of 3.3 equivalents of methyllithium solution (3.1 M, 1.10 mL). The solution was allowed to warm to room temperature by which time the reaction had begun. After 30 minutes, the reaction mixture was cooled to −78 °C before addition of 5 mL of water dropwise. On warming to room temperature, a further 15 mL of water was added to dissolve the newly formed LiCl. The organic layer was separated and stored for later use. The aqueous phase was pH adjusted to neutral before extraction with diethyl ether. The organic fractions were added to the original etherate solution before removal of the solvent under reduced pressure. The resultant brown oil was triturated with petroleum benzine to yield a crude solid. The solid was purified by dissolution into petroleum benzine to yield a white solid (70% yield 0.081 g).

^{1}H NMR (600 MHz, DMSO-d_6) δ = 5.28 (1H, s OH), −0.52 (6H, s, H_{methyl}). Elemental analysis; calcd (%): C 20.6, H 6.04, found: C 20.8, H 6.03.

General procedure 1 (GP1). 1.5 to 3 mmol of the desired hydroxamic acid was dissolved into approximately 20 mL of 50 : 50 ethanol : water before gentle heating to 60 °C. To this, 0.5–1 mmol of the metal nitrate was added to the mixture as a solid. The solution was stirred as $NaHCO_3$ was added dropwise till a pH of approximately 7–8. Visible effervescence of carbon

dioxide was observed as well as precipitation as the pH approached neutral. The white to off-white powders were collected *via* gravity filtration and washed with copious water before air drying.

Synthesis of organometallic complexes 4 and 5. The desired hydroxamic acid, **1** or **2**, 1 mmol or 2 m mmol respectively, was dried under vacuum for approximately 1–2 hours. Dry hexane was added to the Schlenk before cooling to 0 °C in an ice-bath. 1 mmol of neat trimethylgallium was then added by pre-purged syringe to the reaction flask. For complex **5**, the solution was then refluxed for approximately 2 hours after warming to room temperature. The resultant white solids were filtered *via* gravity filtration in the air and washed with cold hexane prior to drying. *Hydroxamic acids*: BPHA-*H* = *N*-benzoyl-*N*-phenylhydroxamic acid, BHA-H_2 = phenylhydroxamic acid, and SHA-H_3 = salicylhydroxamic acid.

[Ga(BPHA)$_3$] 1. 1.5 mmol (0.330 g) of *N*-benzyl-*N*-phenylhydroxamic acid was dissolved into a 50 : 50 mixture of ethanol and water and heated gently to ∼60 °C before the addition of 0.5 mmol (0.209 g) of solid [Ga(NO$_3$)$_3$·9H$_2$O]. NaHCO$_3$ was added dropwise until pH of approximately 7–8. Effervescence of CO_2 was observed. The resultant white precipitate was gravity filtered and washed 3 × 15 mL of H_2O yielding a white solid.

Yield 0.295 g (83%), m.p. 238–242 °C, ^{1}H NMR (600 MHz, DMSO-d$_6$) δ = 7.44–7.29 (30H, m, H$_{ar}$). ^{13}C NMR (151 MHz, DMSO-d$_6$) δ = 162.5 (C═O), 140.7 (C$_{quaternary}$), 130.9 (C$_{ar}$), 130.3 (C$_{ar}$), 129.2 (C$_{ar}$), 128.8 (C$_{ar}$), 128.7 (C$_{ar}$), 128.4 (C$_{ar}$), 126.1 (C$_{ar}$). IR (cm^{-1}): 3053 w ν(C–H$_{ar}$), 1583 w, 1522 s ν(C═O), 1462 m, 1436 m, 1161 s, 760 s, 718 m, 698 s, 669 s. Elemental analysis; calcd (%): C 66.31, H 4.28, N 5.95, found: C 66.16, H 4.21, N 5.82. High-resolution ESI-MS$^+$ *m*/*z*: ([GaC$_{39}$H$_{30}$N$_3$O$_6$ + Na]$^+$) calcd: 728.1282, found: 728.1267. CCDC: 2150403.†

[Ga(BHA-*H*)$_3$] 2. 3.0 mmol (0.430 g) of benzohydroxamic acid was dissolved into a 50 : 50 mixture of ethanol and water and heated gently to ∼60 °C before the addition of 1.0 mmol (0.420 g) of solid [Ga(NO$_3$)$_3$·9H$_2$O]. NaHCO$_3$ was added dropwise until pH of approximately 7–8. Effervescence of CO_2 was observed. The resultant white precipitate was gravity filtered and washed 3 × 15 mL of H_2O yielding a white solid.

Solid state: 82.5% yield (0.28 g, 0.82 mmol) of **2**. m.p. 250 °C (decomp). FT-IR (cm^{-1}): 3371 w ν(N–H), 3194 bw, 3060 w ν(C–H$_{ar}$), 2826 w, 1599 m ν(C═N), 1566 m ν(C═O), 1523 m, 1483 m, 1444 w, 1363 m, 1150 m, 1048 m, 1027 m, 920 s, 781 m, 690 s. Elemental analysis; calcd (%) [**2** + H_2O]: C 46.84, H 3.65, N 7.80, found: C 46.66, H 3.60, N 7.77.

Solution state: ^{1}H NMR (600 MHz, DMSO-d$_6$) δ = 12.79 (3H, bs, NH), 7.80 (6H, d, H$_o$, J = 44 Hz), 7.56 (3H, t, H$_p$, J = 24 Hz), 7.54 (6H, t, H$_m$, J = 28 Hz). ^{13}C NMR (151 MHz, DMSO-d$_6$) δ = 160.1 (C═O), 130.6 (C$_{quaternary}$), 130.70 (C$_{quaternary}$), 128.0 (C$_o$), 127.2 (C$_o$) 126.0 (C$_m$) 124.5 (C$_m$). High resolution ESI-MS$^+$ *m*/*z*: ([GaC$_{14}$H$_{11}$N$_2$O$_4$ + Na]$^+$) calcd: 362.9867, found: 362.9842; ([GaC$_{21}$H$_{18}$N$_3$O$_6$ + Na]$^+$) calcd: 500.0343, found: 500.0310.

[Ga(SHA-H_2)(SHA-*H*)] 3. 3.0 mmol (0.480 g) of salicylhydroxamic acid was dissolved into a 50 : 50 mixture of ethanol and water and heated gently to ∼60 °C before the addition of 1.0 mmol (0.420 g) of solid [Ga(NO$_3$)$_3$·9H$_2$O]. NaHCO$_3$ was added dropwise until pH of approximately 7–8. Effervescence of CO_2 was observed. The resultant pink-white precipitate was gravity filtered and washed 3 × 15 mL of H_2O.

Solid state: Yield 0.27 g (72.7%), m.p. 245 °C (decomp), FT-IR (cm^{-1}): 3065 bw (O–H$_{ph}$), 1599 s ν(C═N), 1569 m ν(C═O), 1512 s, 1475 s, 1364 m, 1304 m, 1247 s, 1147 s, 1096 s, 1033 s, 923 s, 744 s. Elemental analysis; theoretical (%) (**3** + $\frac{1}{2}$H$_2$O): C 44.02, H 3.17, N 7.33. Found: C 44.20, H 3.32, N 7.38. Note: 0.5 equiv. of H_2O observed in TGA trace.

Solution state: [Ga(SHA-H_2)(SHA-*H*)] + [Ga(SHA-H_2)$_3$]: ^{1}H NMR (600 MHz, DMSO-d$_6$) δ = 12.62 (0.12H, d, H$_{im}$), 11.72 (4H, bs, NH/OH), 10.20 (0.05H, bs, H$_{im}$), 9.33 (0.75H, bs, OH$_{ph}$), 7.73 (1H, dd, hydroximate H$_o$), 7.67 (1H, dd, hydroxamate H$_o$), 7.37 (1H, td, hydroxamate H$_p$), 7.32 (1H, td, hydroximate H$_p$), 6.90 (4H, m, hydroximate & hydroxamate H$_m$). ^{13}C NMR (151 MHz, DMSO-d$_6$) δ = 166.2 (C═O), 159.6 (C═N), 159.4 (hydroxamate C$_{quaternary}$), 155.8 (hydroximate C$_{quaternary}$), 133.4 (hydroxamate C$_{phenol}$), 132.3 (hydroximate C$_{phenol}$), 128.5 (hydroximate C$_o$), 127.0 (hydroxamate C$_o$), 119.3 (hydroximate C$_m$), 118.7 (hydroxamate C$_m$), 117.3 (hydroxamate C$_m$), 116.3 (hydroximate C$_m$), 114.2 (hydroximate C$_p$), 114.0 (hydroxamate C$_p$). High resolution ESI-MS$^+$ *m*/*z*: ([GaC$_{14}$H$_{11}$N$_2$O$_6$ + Na]$^+$) calcd: 394.9765, found: 394.9747; ([GaC$_{21}$H$_{18}$N$_3$O$_9$ + Na]$^+$) calcd: 548.0191, found: 548.0166.

[GaMe$_2$(BPHA)] 4. 0.10 mL, 1.00 mmol of trimethyl gallium was added to 0.13 g, 1.00 mmol of dried *N*-benzoyl-*N*-phenylhydroxamic acid suspended in 10 mL of dry hexane under inert conditions at 0 °C. The white suspension was stirred overnight before filtering in air and air drying. Yield 0.208 g (68%), m.p. 99–101 °C. ^{1}H NMR (600 MHz, DMSO-d$_6$) δ = −0.35 (6H, s, CH$_3$), 7.30–7.39 (10H, m, H$_{p,m,o}$). ^{13}C NMR (151 MHz, DMSO-d$_6$) δ = −3.14 (C$_{methyl}$) 18.56 (C$_{methyl\ toluene}$) 125.8 (C$_{ar}$) 127.8 (C$_{ar}$), 127.9 (C$_{ar}$), 128.2 (C$_{ar}$), 128.3 (C$_{ar}$) 128.5 (C$_{ar}$), 128.9 (C$_{ar}$), 130.2 (C$_{ar}$), 130.4 (C$_{ar}$), 131.8 (C$_{ar}$), 141.6 (C$_q$), 163.3 (C═O). FT-IR (cm^{-1}): 3060 b, 2962 b, 2910 ν(C–H), 1586 s (C═O), 1534 s (C–N), 1439 s, 1187 m, 1151 s, 1075 m, 1037 m, 939 s, 914 s, 770 s, 693 s. High resolution ESI-MS$^+$ *m*/*z*: [Ga(CH$_3$)$_2$(C$_6$H$_5$CON(C$_6$H$_5$)O)$_3$ + H] calcd: 312.0513. found: 312.0546. Elemental analysis; calcd (%): C 57.62, H 5.15, N 4.52, found: C 57.74, H 5.17, N 4.49. CCDC: 2380238.†

[GaMe(BHA-*H*)$_2$] 5. 0.10 mL, 1.00 mmol of trimethylgallium was added to 0.286 g, 2.00 mmol of dried benzohydroxamic acid suspended in 10 mL of dry hexane under inert conditions. The white suspension was stirred overnight at reflux before filtering in air and air drying. Yield 0.293 g (82%), m.p.: 262–266 °C (decomp). ^{1}H NMR (600 MHz, DMSO-d$_6$) δ = −0.26 (3H, s, CH$_3$), 7.52 (6H, m, H$_{p,m}$), 4.04 (4H, m, H$_o$), 12.96 (2H, brs, NH). ^{13}C NMR (151 MHz, DMSO-d$_6$) δ = −6.25 (C$_{methyl}$) 21.04 (C$_{methyl\ toluene}$) 125.3 (C$_{ar}$) 126.2 (C$_{ar}$), 128.2 (C$_{ar}$), 128.4 (C$_{ar}$), 128.8 (C$_{ar}$) 128.9 (C$_{ar}$), 131.6 (C), 137.4 (C═O). FT-IR (cm^{-1}): 3193 b, 2848 b (C–H), 2722 b (N–H), 1601 s (C═O), 1535 s (C–N), 1485 m, 1446 w, 1363 w, 1315 w, 1143 s, 1074 s,

1027 m, 923 s, 789 m, 688 s. High resolution ESI-MS$^+$ *m*/*z*: [$GaCH_3(C_6H_5CONHO)_2$ + H] calcd: 357.0361. Found: 357.0358. Elemental analysis (**5** + 0.33 toluene, observed in NMR) calcd (%): C 53.72, H 4.49, N 6.88. Found: C 53.69, H 4.59, N 7.23. CCDC: 2380239.†

[Fe(BPHA)$_3$] 6. NaOH (0.08 g, 2.05 mmol) was added to [BPHA-H_2] (0.42 g, 1.99 mmol) in MeOH (15 mL) in a 100 mL RBF to generate the *in situ* sodium salt. To this, $FeCl_3{\cdot}6H_2O$ (0.29 g, 0.60 mmol) was added, resulting in a dark red solution that was stirred for 20 h at room temperature. The resultant red precipitate was gravity filtered and washed with 3 × 15 mL of MeOH and 3 × 15 mL of H_2O. Red needle-like crystals were obtained from DMSO overnight. Yield 0.30 g (71.7%), m.p. 211 °C. FT-IR (cm^{-1}): 3052 w ν(C–H_{ar}), 2972 w, 2852 w, 1584 w, 1509 s ν(C═O), 1463 m, 1432 s, 1160 m, 1047 m, 1021 m, 938 s, 761 s, 720 m, 693 s, 668 s. Elemental analysis calcd (%): C 67.64, H 4.37, N 6.07, found: C 67.51, H 4.34, N 6.13. High-resolution ESI-MS$^+$ *m*/*z*: ($[FeC_{39}H_{30}N_3O_6 + H]^+$) calcd: 693.1556, found: 693.1557; ($[FeC_{39}H_{30}N_3O_6 + Na]^+$) calcd: 715.1376, found: 715.1375. CCDC: 2150396.†

Author contributions

Professor Phil Andrews: primary investigator and supervisor, writing, editing and revision of manuscript. Dr Rebekah Duffin: data collection, data analysis, research-based activities, writing, editing and revision of manuscript. Equal contribution of authorship. Miss Jenisi Kelderman: data collection, data analysis, research-based activities, writing. Equal contribution of authorship. Dr Megan Herdman: data analysis, research-based activities.

Data availability

The data supporting this article have been included as part of the ESI.†

Crystallographic data for complexes **1–10** have been deposited at the Cambridge Crystallographic Data Centre (CCDC). The relevant CCDC number can be found for each complex in the Experimental sections (incl ESI†).

Conflicts of interest

There are no conflicts to declare.

Acknowledgements

The authors would like to thank the Australian Research Council (DP220103632) and Monash University for financial support. We would also like to thank Dr Craig Forsyth (Monash) for assistance with X-ray crystallography.

References

1 M. Wu and X. Li, *Mol. Med. Microbiol*, Elsevier, 2015, 10, 1547–1564.
2 M. S. Mulani, E. E. Kamble, S. N. Kumkar, M. S. Tawre and K. R. Pardesi, *Front. Microbiol.*, 2019, **10**, 539.
3 R. Podschun and U. Ullmann, *Clin. Microbiol. Rev.*, 1998, **11**, 589–603.
4 C. Schroll, K. B. Barken, K. A. Krogfelt and C. Struve, *BMC Microbiol.*, 2010, **10**, 1–10.
5 J. Jagnow and S. Clegg, *Microbiology*, 2003, **149**, 2397–2405.
6 L. S. Munoz-Price, L. Poirel, R. A. Bonomo, M. J. Schwaber, G. L. Daikos, M. Cormican, G. Cornaglia, J. Garau, M. Gniadkowski and M. K. Hayden, *Lancet Infect. Dis.*, 2013, **13**, 785–796.
7 K. Kuo, Y. Shen and K. Hwang, *J. Microbiol. Immunol. Infect.*, 2007, **40**, 248–254.
8 G. Cortés, N. Borrell, B. de Astorza, C. Gómez, J. Sauleda and S. Albertí, *Infect. Immun.*, 2002, **70**, 2583–2590.
9 H. Sahly, R. Podschun, T. A. Oelschlaeger, M. Greiwe, H. Parolis, D. Hasty, J. R. Kekow, U. Ullmann, I. Ofek and S. Sela, *Infect. Immun.*, 2000, **68**, 6744–6749.
10 E. Padilla, E. Llobet, A. Doménech-Sánchez, L. Martínez-Martínez, J. A. Bengoechea and S. Albertí, *Antimicrob. Agents Chemother.*, 2010, **54**, 177–183.
11 B. Li, Y. Zhao, C. Liu, Z. Chen and D. Zhou, *Future Microbiol.*, 2014, **9**, 1071–1081.
12 T. A. Russo, A. S. Shon, J. M. Beanan, R. Olson, U. MacDonald, A. O. Pomakov and M. P. Visitacion, *PLoS One*, 2011, **6**, e26734.
13 M. A. Bachman, S. Lenio, L. Schmidt, J. E. Oyler and J. N. Weiser, *mBio*, 2012, **3**, e00224–e00211.
14 M. A. Bachman, J. E. Oyler, S. H. Burns, M. Caza, F. Lépine, C. M. Dozois and J. N. Weiser, *Infect. Immun.*, 2011, **79**, 3309–3316.
15 D. C. Bailey, E. J. Drake, T. D. Grant and A. M. Gulick, *Biochemistry*, 2016, **55**, 3559–3570.
16 M. A. Bachman, V. L. Miller and J. N. Weiser, *PLoS Pathog.*, 2009, **5**, e1000622.
17 C. R. Chitambar, *Biochim. Biophys. Acta, Mol. Cell Res.*, 2016, **1863**, 2044–2053.
18 A. B. Kelson, M. Carnevali and V. Truong-Le, *Curr. Opin. Pharmacol.*, 2013, **13**, 707–716.
19 J. A. A. Huayhuaz, H. A. Vitorino, O. S. Campos, S. H. P. Serrano, T. M. Kaneko and B. P. Espósito, *J. Trace Elem. Med. Biol.*, 2017, **41**, 16–22.
20 T. Sultana, R. N. Duffin, V. L. Blair and P. C. Andrews, *Chem. Commun.*, 2023, **59**, 11093–11096.
21 R. N. Duffin and P. C. Andrews, *J. Inorg. Biochem.*, 2023, **249**, 112371.
22 R. N. Duffin, V. L. Blair, L. Kedzierski and P. C. Andrews, *Eur. J. Med. Chem.*, 2020, **186**, 111895.
23 M. J. McKeage, S. J. Berners-Price, P. Galettis, R. J. Bowen, W. Brouwer, L. Ding, L. Zhuang and B. C. Baguley, *Cancer Chemother. Pharmacol.*, 2000, **46**, 343–350.

24 T. Riss and R. Moravec, *Assay Drug Dev. Technol.*, 2004, **2**, 51–62.
25 R. S. Go and A. A. Adjei, *J. Clin. Oncol.*, 1999, **17**, 409–422.
26 Y. He, Q. Zhu, M. Chen, Q. Huang, W. Wang, Q. Li, Y. Huang and W. Di, *Oncotarget*, 2016, **7**, 70803–70821.
27 Y. T. Wang, Y. Fang, M. Zhao, M. X. Li, Y. M. Ji and Q. X. Han, *MedChemComm*, 2017, **8**, 2125–2132.
28 C. Y. Effah, T. Sun, S. Liu and Y. Wu, *Ann. Clin. Microbiol. Antimicrob.*, 2020, **19**, 1–9.
29 S. Hijazi, D. Visaggio, M. Pirolo, E. Frangipani, L. Bernstein and P. Visca, *Front. Cell. Infect. Microbiol.*, 2018, **8**, 316.
30 C. R. Chitambar, D. P. Purpi, J. Woodliff, M. Yang and J. P. Wereley, *J. Pharmacol. Exp. Ther.*, 2007, **322**, 1228–1236.
31 L. R. Bernstein, T. Tanner, C. Godfrey and B. Noll, *Met.-Based Drugs*, 2000, **7**, 33–47.
32 D. K. Coggin, C. J. Mathias and M. A. Green, *Nucl. Med. Biol.*, 1994, **21**, 283–285.
33 C. R. Chitambar and Z. Zivkovic, *Cancer Res.*, 1987, **47**, 3929–3934.
34 W. R. Harris and L. Messori, *Coord. Chem. Rev.*, 2002, **228**, 237–262.
35 W. R. Harris and V. L. Pecoraro, *Biochemistry*, 1983, **22**, 292–299.
36 É. A. Enyedy, O. Dömötör, K. Bali, A. Hetényi, T. Tuccinardi and B. K. Keppler, *J. Biol. Inorg. Chem.*, 2015, **20**, 77–88.
37 G. M. Sheldrick, *Acta Crystallogr., Sect. A: Found. Adv.*, 2008, **64**, 112–122.
38 O. V. Dolomanov, L. J. Bourhis, R. J. Gildea, J. A. Howard and H. Puschmann, *J. Appl. Crystallogr.*, 2009, **42**, 339–341.
39 R. N. Duffin, V. L. Blair, L. Kedzierski and P. C. Andrews, *Dalton Trans.*, 2018, **47**, 971–980.
40 R. N. Duffin, V. L. Blair, L. Kedzierski and P. C. Andrews, *J. Inorg. Biochem.*, 2018, **189**, 151–162.
41 R. N. Duffin, V. L. Blair, L. Kedzierski and P. C. Andrews, *J. Inorg. Biochem.*, 2020, **203**, 110932.
42 R. N. Duffin, V. L. Blair, L. Kedzierski and P. C. Andrews, *J. Inorg. Biochem.*, 2021, **219**, 111385.
43 A. Pathak, V. L. Blair, R. L. Ferrero, L. Kedzierski and P. C. Andrews, *J. Inorg. Biochem.*, 2017, **177**, 266–275.
44 M. Werrett, M. Herdman, R. Brammananth, U. Garusinghe, W. Batchelor, P. Crellin, R. Coppel and P. C. Andrews, *Chem. – Eur. J.*, 2018, **24**, 12938–12949.